

Neutron scattering studies of the paramagnetic response in the mixed-valence alloy $\text{Ce}_{1-x}\text{Th}_x$ at high energy

C.-K. Loong

Intense Pulsed Neutron Source, Argonne National Laboratory, Argonne, Illinois 60439

B. H. Grier

Physics Department, West Virginia University, Morgantown, West Virginia 26506

S. M. Shapiro

Physics Department, Brookhaven National Laboratory, Upton, New York 11973

J. M. Lawrence

Physics Department, University of California-Irvine, Irvine, California 92717

R. D. Parks*

Physics Department, New York University, New York, New York 10003

S. K. Sinha

Exxon Research and Engineering Co., Corporate Research Laboratories, Annandale, New Jersey 08801

(Received 25 September 1986)

We report on the inelastic neutron scattering investigations of the cerium $\gamma \leftrightarrow \alpha$ valence transition in $\text{Ce}_{0.74}\text{Th}_{0.26}$ at energy transfers up to ~ 500 meV. The paramagnetic response across the transition was studied in detail at five temperatures between 10 and 200 K. The obtained magnetic scattering functions consist of a broad peak with a line shape consistent with a generalized relaxational spin dynamics. As the temperature decreases across the transition the magnetic intensity drops sharply, accompanied by an abrupt broadening of the linewidth corresponding to a spin-fluctuation energy much higher than the thermal energy. Within experimental precision, we find no evidence of additional inelastic peaks due to crystal-field excitations. The static single-site susceptibility obtained by a Kramers-Kronig analysis agrees well with the bulk susceptibility. The comparison of the present results with analysis in terms of a "dense impurity" model of the f electron in hybridization with the conduction-band states is discussed.

I. INTRODUCTION

The physics of the $\gamma \rightarrow \alpha$ phase transition in Ce metal has been the subject of numerous experimental and theoretical investigations.¹⁻¹⁷ Many different models for the mechanism driving this phase transition have been proposed. These range from models involving promotion or delocalization of the $4f$ electron into a conduction-band state to models involving a change in the Kondo condensation energy association with a change in volume and in the f -electron-conduction-electron hybridization. The former models necessarily involve a significant change in the electronic structure, and in particular, of the f -electron occupation n_f across the transition, while the latter models imply that n_f changes only slightly and is large (≤ 1) in both phases. Evidence from electronic spectroscopy measurements,¹³⁻¹⁶ as well as Compton scattering¹⁷ and positron annihilation measurements¹² indicates that n_f undergoes a relatively minor change at the phase transition. The results of electronic spectroscopy experiments have been quantitatively fitted¹⁸ in terms of a model due to Gunnarsson and Schönhammer¹⁹ and parameters suitably chosen to represent the hybridization, the conduction-band width, the bare f level, and the spin-

orbit splitting, respectively. Reasonable agreement is obtained with experiment for both the γ and α phases of cerium. Very similar theoretical models to explain the electronic spectroscopy results have been presented by other authors.²⁰ Practically all the dynamical information contained in electronic spectroscopy experiments involves matrix elements coupling the ground state to excited states, often with a hole in the latter, as in photoemission experiments. Such experiments involve quantities such as the single- $4f$ -electron spectral density function. Inelastic neutron scattering involves a rather different low-frequency spectroscopy, namely, the measurement of the frequency dependence (and in principle, also the wave-vector dependence) of the dynamical magnetic susceptibility. While the calculation of this quantity for systems with strong Coulomb correlations is a complicated business, compared to the calculation of one-electron properties, it does have the advantage of being able to probe low-lying excitations above the ground state with relatively good energy resolution. It is thus of interest to examine to what extent the results of such experiments are consistent with models which explain the electronic spectroscopy data.

In pure cerium metal, the $\gamma \rightarrow \alpha$ transition is complicat-

ed by the existence of the β phase at ambient pressure. However, one may study the same transition as a function of temperature by alloying cerium with thorium.²¹ The physical behavior of the alloy system $Ce_{1-x}Th_x$, in particular that related to the $\gamma \rightarrow \alpha$ transition and the spin fluctuations, has been studied extensively.^{22,23} Lawrence *et al.*²² showed that there is a critical concentration of thorium at which the transition becomes second order. In an earlier study using thermal neutrons, Shapiro *et al.*²⁴ have measured the temperature dependence of the magnetic response of the alloy $Ce_{0.74}Th_{0.26}$ across the $\gamma \rightarrow \alpha$ transition. At this concentration, which is close to the critical concentration, the transition is still first order. They observed only a quasielastic component in the magnetic scattering function $S_{\text{mag}}(\mathbf{Q}, E)$ which displays an abrupt broadening and decreases in intensity as the temperature drops below the transition temperature T_0 . While they were able to characterize the scattering in the γ phase ($T > T_0$) fairly well, and were able to demonstrate that it arose predominantly from f electrons (by examining the dependence of the intensity on $|\mathbf{Q}|$), the scattering in the α phase ($T < T_0$) was so broad that they were unable to characterize its width or its Q dependence definitively.

In recent years, the advent of pulsed spallation neutron sources and the installation of hot moderators at steady-state reactors have made possible neutron scattering studies of elementary excitations at energies up to hundreds of meV.^{25,26} In this paper, we report on the inelastic neutron scattering investigations of the $\gamma \rightarrow \alpha$ transition in $Ce_{0.74}Th_{0.26}$, an alloy with concentration identical to that studied by Shapiro *et al.*,²⁴ using the pulsed spallation source [Intense Pulsed Neutron Source (IPNS)] of Argonne National Laboratory. Due to the unavailability of large enough single crystals, a polycrystalline sample was used. The momentum-space resolution was such that, together with the polycrystalline averaging, the scattering at a given energy transfer E was averaged over all \mathbf{q} in the Brillouin zone. Thus, of necessity, q -dependent effects such as coherence effects between the f electrons cannot be studied in such an experiment. The data are thus analyzed in terms of a "dense impurity" model of the f electrons, as is done in practically all theoretical treatments and in the electronic spectroscopy measurements. It should be borne in mind, however, that in principle neutron scattering measurements on single crystals can shed light on the important question of impurity versus coherence effects.

The plan of this paper is as follows. In Sec. II, we give a brief description of the chopper spectrometers at IPNS on which the experiments were carried out, and of the samples used. Since the extraction of the magnetic contribution to the observed scattering intensity is of crucial importance, we describe the methods used in more detail in Sec. III. In Sec. IV, we discuss the momentum and energy dependence of the magnetic scattering in both phases. Section V contains a summary and a discussion of the results.

II. EXPERIMENTAL PROCEDURE

The experiments were performed on the Low-Resolution (LRMECS) and High-Resolution (HRMECS)

Medium-Energy Chopper Spectrometers²⁷ at IPNS. A schematic drawing of the instruments is shown in Fig. 1(a). A Fermi chopper phased to the pulsed neutron source produces pulses of monochromatic neutrons which are incident on the sample. The momentum and energy transfers (\mathbf{Q}, E) are determined by neutron time-of-flight techniques in over 140 detectors covering scattering angles from -10° to 120° for LRMECS and over 200 detectors from -15° to 20° for HRMECS. [The scattering angle is taken as positive in the sense shown in Fig. 1(a).] A variety of choppers have been designed to select neutrons of energies ranging from about 30 meV to 2 eV. The energy resolution in general depends on the chopper in use and varies with energy transfer but is approximately 6–8% of the incident energy E_0 for LRMECS and 2–5% for HRMECS. As can be seen in Fig. 1(b), the use of a chopper spectrometer enables us to survey the scattering function over a wide range of momentum and energy transfer. Although data obtained with $E_0 = 500$ meV on $Ce_{0.74}Th_{0.26}$ from the early period of LRMECS operation

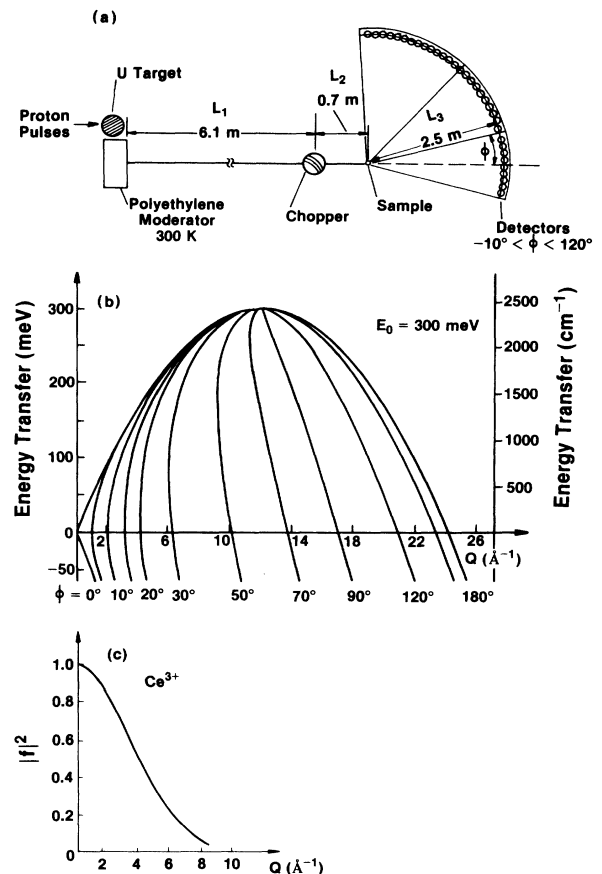


FIG. 1. (a) Schematic drawing of the IPNS Low-Resolution Medium-Energy Chopper Spectrometer (LRMECS). The layout of HRMECS is similar, with instrumental parameters $L_1 = 12.7$ m, $L_2 = 1.2$ m, $L_3 = 4$ m, $-15^\circ < \phi < 20^\circ$ and $80^\circ < \phi < 140^\circ$. (b) Parabolic loci in (Q, E) space for detectors at fixed angles corresponding to the operation of a chopper spectrometer with an incident energy of 300 meV. (c) The Q dependence of the neutron magnetic form factor for a tripositive cerium free ion.

indicated an abrupt change in the paramagnetic response at temperatures near the cerium $\gamma \rightarrow \alpha$ phase transition, severe background problems hindered a quantitative analysis of the dynamical spin susceptibility. Subsequently, we have improved the shielding in the flight-path chamber of the spectrometer and have drastically reduced background scattering to a minimal level. The results presented here correspond to a series of recent measurements made under the upgraded conditions with incident neutron energies of 300 meV on LRMECS and 1200 meV on HRMECS. Preliminary results of these investigations were reported in an earlier paper.²⁵

Polycrystalline samples of $\text{Ce}_{0.74}\text{Th}_{0.26}$ (144 g) and $\text{La}_{0.74}\text{Th}_{0.26}$ (134 g) in the form of small buttons of thickness ~ 0.6 cm and diameter ~ 1.5 cm were prepared using a method described elsewhere.²⁴ The specimen was contained in an aluminum cell in the shape of a thin slab. The slab was mounted at a 45° angle with the incident neutron beam (of dimension $5 \times 10 \text{ cm}^2$) so that for all detector angles the beam did not traverse more than 1 cm of material. Such a geometry minimizes multiple scattering of the neutrons. A Displex refrigerator was employed to cool the sample and the sample temperature was controlled to within about 0.5 K. The measurements consisted of runs for $\text{Ce}_{0.74}\text{Th}_{0.26}$ at 10, 100, 140, 155, and 200 K; $\text{La}_{0.74}\text{Th}_{0.26}$ at 10, 100, and 200 K; sample container at 10 and 150 K; a slab of neutron absorber made of B_4C powder at 100 K; and a thin plate of vanadium at 296 K. The container and absorber runs were used to correct for background scattering and to assess the effect of sample attenuation. The measurements of elastic incoherent scattering from vanadium provided detector calibration and intensity normalization²⁸ to absolute units for scattering cross section.

III. RESULTS AND ANALYSIS

The measured spectrum of $\text{Ce}_{0.74}\text{Th}_{0.26}$ consists of the elastic and inelastic components of both magnetic and nuclear scattering. Therefore, a reliable extraction of the magnetic component from the observed intensity is crucial in the present measurements. Due to the finite extent of the spatial distribution of the electrons contributing to the scattering process, the intensity of magnetic scattering is modulated by the square of the neutron magnetic form factor, $|f(\mathbf{Q})|^2$, which falls off rapidly as the neutron momentum transfer \mathbf{Q} increases. Figure 1(c) shows the Q dependence of the magnetic form factor²⁹ of the Ce^{3+} free ion. Consequently, at large Q ($> 8 \text{ \AA}^{-1}$) nuclear scattering is the sole constituent of the measured spectrum. This feature provides a means for a consistency check of the overall results.

To obtain quantitative information about elastic and inelastic contributions from nuclear scattering in $\text{Ce}_{0.74}\text{Th}_{0.26}$, we have measured, under identical experimental conditions, the energy spectrum of the isostructural alloy $\text{La}_{0.74}\text{Th}_{0.26}$. Since La and Ce have comparable masses and similar ($5d6s^2$) outer electronic configurations (of course, La, unlike Ce, does not have any $4f$ electrons), one would expect identical phonon contribution in these two alloys, apart from the difference in the scattering

lengths, in the absence of strong electron-phonon coupling involving the f shells. Such effects are usually restricted to a relatively small number (if any) of the phonon modes and consequently would not be expected to make dramatic differences in a polycrystalline-average phonon spectrum as measured in these experiments. In any case, as we shall see, the present data, which are analyzed assuming identical phonon spectra, yield a consistently smooth additional magnetic contribution for $\text{Ce}_{0.74}\text{Th}_{0.26}$, indicating the reasonableness of this assumption. Figure 2 displays the scattered intensity from 40 to 200 meV of these two materials at 100 K taken at a scattering angle of 4.2° . The $\text{La}_{0.74}\text{Th}_{0.26}$ [Fig. 2(b)] spectrum exhibits significant one-phonon and multiphonon scattering up to about 80 meV. The broad peak at about 110 meV is attributed to scattering from impurities in the sample. It is well known²⁴ that in our nominally pure sample, it is difficult to avoid a small content of interstitial hydrogen and oxygen below the level of about 1%. In fact, we observed extra scattering in both the $\text{Ce}_{0.74}\text{Th}_{0.26}$ and $\text{La}_{0.74}\text{Th}_{0.26}$ samples at approximately 110 and 220 meV at all angles with intensity distribution consistent with that expected for localized vibrational modes (fundamental and first harmonic) of interstitial hydrogen atoms in the alloys. The spectrum of $\text{Ce}_{0.74}\text{Th}_{0.26}$ [Fig. 2(a)], on the other hand, shows excess scattering extending up to about 200 meV. That this additional component is magnetic in origin was established by the rapid decrease in intensity with increasing Q in accordance with the square of the magnetic form factor.

In order to isolate the paramagnetic scattering in $\text{Ce}_{0.74}\text{Th}_{0.26}$, various contributions from nuclear scattering must be subtracted. We have adopted two approaches in doing that. The first method is to assess the nuclear scattering components, namely, nuclear Bragg reflections, nuclear spin incoherent scattering, phonons, and hydrogen

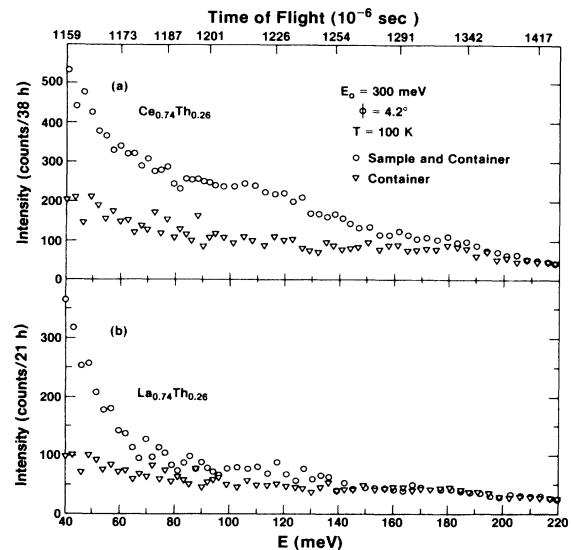


FIG. 2. Time-of-flight data for (a) the $\text{Ce}_{0.74}\text{Th}_{0.26}$ and (b) the $\text{La}_{0.74}\text{Th}_{0.26}$ runs at scattering angle of 4.2° . Data within the time channels corresponding to about 6 meV were averaged over to improve statistics.

localized vibrations, by fitting the energy spectra of the nonmagnetic $\text{La}_{0.74}\text{Th}_{0.26}$. For this purpose, a series of Gaussian functions in energy, convoluted with the instrumental resolution, was used to fit the $\text{La}_{0.74}\text{Th}_{0.26}$ spectrum. Once the parameters for all these contributions are determined, they are used, together with an additional magnetic spectral function, to fit the measured spectra of $\text{Ce}_{0.74}\text{Th}_{0.26}$. The second approach is to multiply the $\text{La}_{0.74}\text{Th}_{0.26}$ data by a scaling factor to account for the different cross sections of Ce and La, thereby obtaining a representative nuclear scattering component for $\text{Ce}_{0.74}\text{Th}_{0.26}$. The magnetic part in the $\text{Ce}_{0.74}\text{Th}_{0.26}$ is then obtained by subtracting off the scaled data. We estimated that these subtraction procedures can yield an error of up to $\sim 20\%$ in the deduced magnetic spectral response. The major uncertainty arises from the effects of multiple Bragg scattering and from the nuclear-spin incoherent scattering of La, which have not been taken into account accurately in the analysis. These effects, however, in general only have significant influence on the data within the elastic region of the spectrum (e.g., $|E| < 40$ meV for $E_0 = 300$ meV). On the other hand, more reliable data at energies below 50 meV have already been obtained in the previous study.²⁴ The present experiment is aimed at the determination of the magnetic susceptibility of $\text{Ce}_{0.74}\text{Th}_{0.26}$ at high-energy transfers.

Figures 3(a) and 3(b) show the energy spectra of $\text{Ce}_{0.74}\text{Th}_{0.26}$ and $\text{La}_{0.74}\text{Th}_{0.26}$ at 100 K measured at a scattering angle of 92° . Here, Q varies from 14 to 18 \AA^{-1} . Therefore, we expect only contributions from nuclear scattering. As would be expected, the observed spectra of the two alloys are quite similar. We find that they both can be fitted well by Gaussian functions convoluted with the instrumental resolution. Note that the two peaks at 108 and 222 meV, corresponding, respectively, to the fundamental and the first-harmonic local modes of H, are clearly evident. At smaller scattering angles correspond-

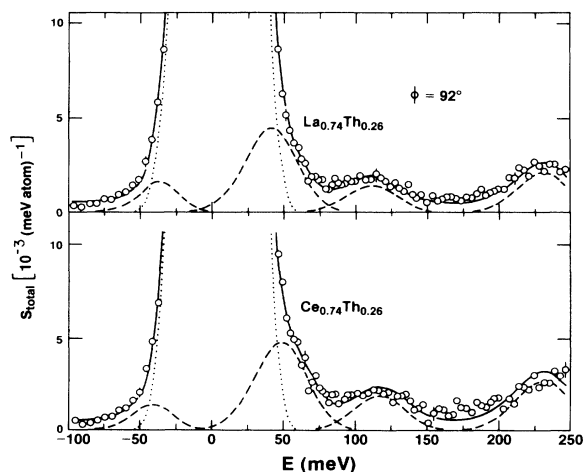


FIG. 3. Energy spectrum at $\phi = 92^\circ$ for (a) $\text{La}_{0.74}\text{Th}_{0.26}$ and (b) $\text{Ce}_{0.74}\text{Th}_{0.26}$ at 100 K. Data points represent the measured total scattering function. Solid curves were obtained by fitting the data with Gaussian phonon and hydrogen peaks (dashed curves) and nuclear elastic peaks (dotted curves).

ing to lower Q values (see Fig. 4 where $\phi = 3.5^\circ$ and $1 < Q < 5 \text{ \AA}^{-1}$), the phonon and H mode intensities decrease according to the behavior expected for lattice and localized vibrations. Magnetic scattering in $\text{Ce}_{0.74}\text{Th}_{0.26}$, on the other hand, becomes the dominant part because of the increasing magnetic form factor. The temperature dependence of the paramagnetic response of $\text{Ce}_{0.74}\text{Th}_{0.26}$ obtained by the two methods described above is shown in Figs. 5 and 6. It can be seen in Fig. 5 that both subtraction procedures arrived at the same results at 100 and 200 K. Data for $E < 40$ meV obtained by the second subtraction method are not presented here because of the aforementioned reasons, namely, the large uncertainties in multiple Bragg scattering and in nuclear-spin incoherent scattering of La within the elastic region. We find that at temperatures between 100 and 200 K the derived magnetic component of $\text{Ce}_{0.74}\text{Th}_{0.26}$ consists of a broad quasielastic peak with significant intensity extended to energies above 100 meV. The magnetic scattering in $\text{Ce}_{0.74}\text{Th}_{0.26}$ at 10 K derived from the second subtraction scheme is shown in Fig. 6. With an incident neutron energy at 1200 meV, the HRMECS runs aimed at the determination of the magnetic response over a wider range of energy transfer up to about 500 meV. (Data at $E > 500$ meV, corresponding to $Q > 6 \text{ \AA}^{-1}$, cannot be accurately determined because of the vanishing form factor.) We find that at 10 K the magnetic scattering is dominated by an inelastic component which exhibits a broad maximum at about 150 meV and a long tail up to about 500 meV.

To give further credence to the magnetic origin of the final result, we have examined the magnetic component over the entire measured (Q, E) space. We find that the magnetic scattering at all temperatures falls off smoothly as a function of Q which is characteristic of a magnetic form factor behavior. Figure 7 displays the data points of adjacent detectors at fixed energies. The solid curves were obtained by least-squares fits of the square of the Ce^{3+}

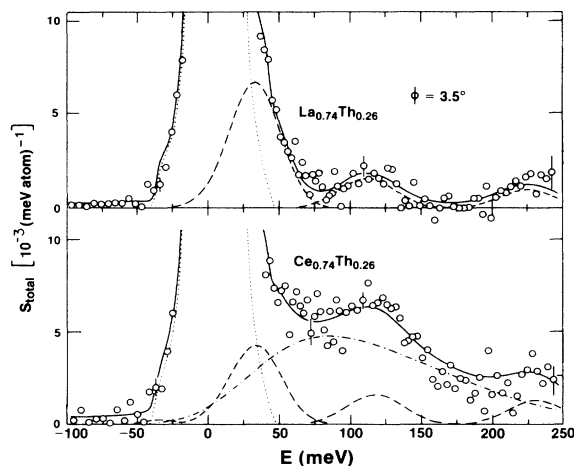


FIG. 4. Energy spectrum at $\phi = 3.5^\circ$ for (a) $\text{La}_{0.74}\text{Th}_{0.26}$ and (b) $\text{Ce}_{0.74}\text{Th}_{0.26}$ at 100 K. The Legends are the same as in Fig. 3. In addition, the magnetic response function given by Eq. (9) is designated by the chain-dotted curve.

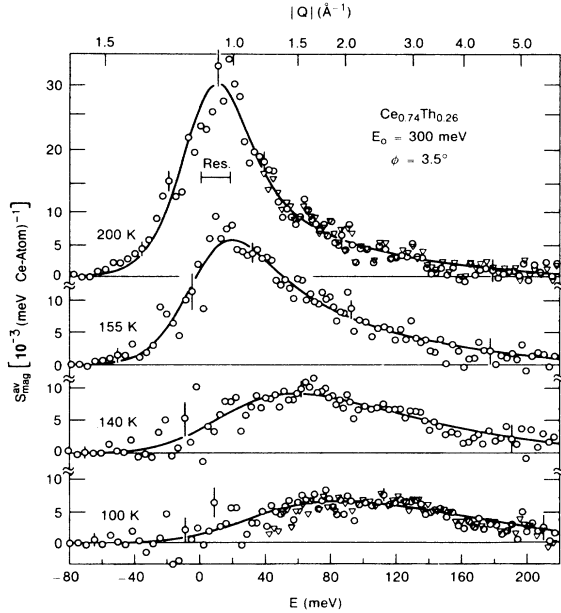


FIG. 5. Temperature dependence of the derived magnetic scattering function, $S_{\text{mag}}^{\text{av}}$, for $\text{Ce}_{0.74}\text{Th}_{0.26}$. The circles and the triangles are data points obtained by subtraction methods 1 and 2, respectively (see text). The solid curves represent the results of fitting the data obtained by method 1 with the scattering function given in Eq. (10) with $B(T)=0$, i.e., a quasielastic line only.

ionic form factor²⁹ to the data sets. As can be seen, the magnetic scattering in $\text{Ce}_{0.74}\text{Th}_{0.26}$ at both 100 and 200 K has a Q dependence determined by the magnetic form fac-

$$S_{\text{mag}}(\mathbf{Q}, E) = \frac{1}{\hbar} |f(\mathbf{Q})|^2 g_J^2 \frac{1}{\pi} \sum_{i,j} e^{i\mathbf{q} \cdot (\mathbf{R}_i - \mathbf{R}_j)} \int_{-\infty}^{+\infty} dt e^{-iEt/\hbar} \langle J_i^\alpha(0) J_j^\alpha(t) \rangle, \quad (2)$$

where $f(\mathbf{Q})$ is the f -shell form factor, g_J is the Landé g factor for f shell, \mathbf{q} is \mathbf{Q} reduced to the first Brillouin zone, and the sum is over all lattice sites $\mathbf{R}_i, \mathbf{R}_j$. α is any

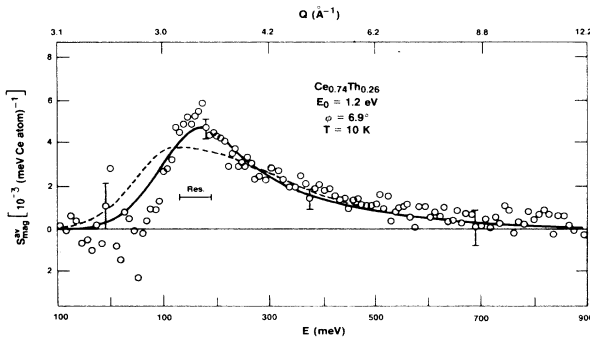


FIG. 6. Magnetic scattering function for $\text{Ce}_{0.74}\text{Th}_{0.26}$ at 10 K obtained by subtraction method 2. The solid curve was obtained by fitting the data by an inelastic Lorentzian function given by Eq. (10) with $A(T)=0$ (see Table I). The dashed curve represents the result of fitting the data by a quasielastic peak [$B(T)=0$].

tor. While confirming the magnetic origin of the extra scattering in $\text{Ce}_{0.74}\text{Th}_{0.26}$, these results, however, yield no information regarding collective or interaction effects in $\chi(\mathbf{Q}, E)$. This is because such effects would manifest themselves as a dependence of \mathbf{q} , the wave vector reduced to the first Brillouin zone. However, the resolution of the experiment, together with the polycrystalline averaging implicit in the scattering, ensures that all points within the Brillouin zone are averaged over in our experiment. As was mentioned before, throughout the data analysis, the scattering cross section has been put into an absolute scale in units of mb per meV per steradian per atom.

IV. ANALYSIS OF THE DATA

The analysis presented in the preceding section indicates that the magnetic scattering observed in the Q ranges accessible to the experiment is predominantly from the f shell. This is true for the scattering in both the γ and α phases. The double-differential magnetic scattering cross section for neutron energy loss E and momentum transfer $\hbar\mathbf{Q}$ from an isotropic paramagnetic system of f electrons in zero external field is, for the case of unpolarized neutrons, given by^{30,31}

$$\frac{d^2\sigma}{d\Omega dE} = \frac{k_f}{k_i} \frac{(\gamma r_e)^2}{4} S_{\text{mag}}(\mathbf{Q}, E), \quad (1)$$

where k_i, k_f are, respectively, the magnitudes of the incident and scattered neutron wave vector, γ is the magnetic moment of the neutron in Bohr magnetons, r_e is the classical electron radius (equal to 2.8×10^{-13} cm), and $S_{\text{mag}}(\mathbf{Q}, E)$ is given by

Cartesian component for the angular momentum \mathbf{J} on the site i .

Since we are studying $S_{\text{mag}}(\mathbf{Q}, E)$ for a polycrystalline specimen and with a \mathbf{Q} resolution (e.g., $\Delta|\mathbf{Q}|/|\mathbf{Q}| \sim 3\%$ at $\phi=3.5^\circ$, $E=100$ meV, $|\mathbf{Q}|=2.3 \text{ \AA}^{-1}$) comparable to the size of a Brillouin zone, we replace $S_{\text{mag}}(\mathbf{Q}, E)$ by $S_{\text{mag}}^{\text{av}}(Q, E)$, its average over all \mathbf{q} in the Brillouin zone. This leads to

$$S_{\text{mag}}^{\text{av}}(Q, E) = \frac{1}{\hbar} |f(Q)|^2 g_J^2 \frac{1}{\pi} \sum_i \int_{-\infty}^{+\infty} dt e^{iEt/\hbar} \times \langle J_i^\alpha(0) J_i^\alpha(t) \rangle, \quad (3)$$

which may in turn be related to the average dynamical susceptibility $\chi(E, T)$ for an f electron on a *single site*, by the relation

$$\begin{aligned} & \frac{1}{2\pi\hbar} \int_{-\infty}^{+\infty} dt e^{iEt/\hbar} \langle J_i^\alpha(0) J_i^\alpha(t) \rangle \\ &= \frac{(1 - e^{-E/k_B T})^{-1}}{\pi g_J^2 \mu_B^2} \text{Im}\chi(E, T), \quad (4) \end{aligned}$$

TABLE I. The half-widths Γ and the static single-site susceptibility χ_0 obtained from least-squares fits of the neutron data. χ_{bulk} is the measured bulk susceptibility for a $\text{Ce}_{0.731}\text{Th}_{0.269}$ sample.²⁴

T (K)	Γ_1 (meV)	Γ_2 (meV)	ξ (meV)	χ_0 (10^{-3} emu/mole Ce)	χ_{bulk}
10		86.7 \pm 5	138.6 \pm 6	0.333 \pm 0.02	0.54 \pm 0.07
100	110.0 \pm 6			0.831 \pm 0.05	
140	62.6 \pm 4			1.107 \pm 0.07	1.02 \pm 0.06
155	24.6 \pm 2			1.845 \pm 0.11	2.21 \pm 0.05
200	15.9 \pm 1			1.957 \pm 0.12	2.34 \pm 0.05

where k_B is Boltzmann's constant and T is the temperature. From Eqs. (3) and (4) we have

$$S_{\text{mag}}^{\text{av}}(Q, E) = \frac{2N}{\pi\mu_B^2} |f(Q)|^2 (1 - e^{-E/k_B T})^{-1} \text{Im}\chi(E, T), \quad (5)$$

N being the total number of sites. Note that, because of the \mathbf{q} averaging, we are not studying the total dynamical susceptibility $\text{Im}\chi(\mathbf{q}, E, T)$ of the whole system, but rather the *single-site susceptibility*. These will be proportional to one another in so far as the individual f -electron sites are *noninteracting*, but it is important to emphasize what is rigorously measured in the experiment. [In Eq. (5), the Debye-Waller factor in the cross section has been neglected, since it is essentially unity for the Q values and temperatures studied in the present experiment.] Figures 5 and 6 show $S_{\text{mag}}^{\text{av}}(Q, E)$ as measured in the present experiment.

The quantity $\text{Im}\chi(E, T)$ obeys two important sum rules. One follows from Eq. (4), namely,

$$\begin{aligned} \int_{-\infty}^{+\infty} dE (1 - e^{-E/k_B T})^{-1} \text{Im}\chi(E, T) \\ = \pi g_J^2 \mu_B^2 \langle [J_i^z(0)]^2 \rangle \\ = \frac{\pi}{3} g_J^2 \mu_B^2 J(J+1) \langle n_f \rangle, \end{aligned} \quad (6)$$

where $\langle n_f \rangle$ is the average f occupation per site of the lattice. The other follows from the Kramers-Kronig relation,

$$\frac{1}{\pi} \int_{-\infty}^{+\infty} dE \frac{\text{Im}\chi(E, T)}{E} = \chi_0(T), \quad (7)$$

where $\chi_0(T)$ is the *static single-site* susceptibility. Because of Eq. (7), it is often convenient to write

$$\text{Im}\chi(E, T) = \pi E \chi_0(T) P(E, T), \quad (8)$$

where $P(E, T)$ is a dynamical spectral function. There is currently no analytical form for $P(E, T)$. A commonly used representation^{23,30} is the generalized Lorentzian form

$$\begin{aligned} P(E, T) = \frac{1}{\pi} \left[\frac{A(T)\Gamma_1(T)}{[\Gamma_1(T)]^2 + E^2} + \frac{B(T)\Gamma_2(T)}{[\Gamma_2(T)]^2 + (E - \xi)^2} \right. \\ \left. + \frac{B(T)\Gamma_2(T)}{[\Gamma_2(T)]^2 + (E + \xi)^2} \right]. \end{aligned} \quad (9)$$

In terms of this function, the magnetic scattering function can be written as

$$\begin{aligned} S_{\text{mag}}^{\text{av}}(Q, E) = 2N \frac{\chi_0(T)}{\mu_B^2} |f(Q)|^2 (1 - e^{-E/k_B T})^{-1} E \frac{1}{\pi} \\ \times \left[\frac{A(T)\Gamma_1(T)}{[\Gamma_1(T)]^2 + E^2} + \frac{B(T)\Gamma_2(T)}{[\Gamma_2(T)]^2 + (E - \xi)^2} \right], \end{aligned} \quad (10)$$

where the Lorentzian at $E = -\xi$ has been neglected because of the vanishingly small detailed balance factor for $E < 0 < k_B T$. The results of using such a function to fit the measured spectra at $200 \leq T \leq 100$ K and at $T = 10$ K are shown (by the solid curves) in Figs. 5 and 6, respectively. In the least-squares analysis, the magnetic form factor²⁹ of the Ce^{3+} free ion was used. At $200 \leq T \leq 100$ K we assumed only a quasielastic component [i.e., $B(T) = 0$], whereas in the case of $T = 10$ K we allowed for an *inelastic* Lorentzian centered at ξ only [$A(T) = 0$]. These procedures helped limit the fits to not more than

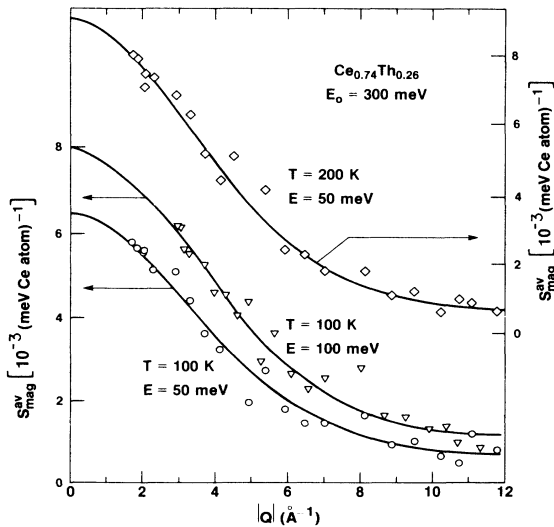


FIG. 7. Magnetic scattering function of $\text{Ce}_{0.74}\text{Th}_{0.26}$ at 100 and 200 K obtained by method 2 (see text) is displayed at fixed energies. The solid curves represent the results of fitting the square of the Ce^{3+} $4f$ form factor to the data sets.

three adjustable parameters. The functional form (10) is seen to provide a satisfactory fit to the data at all temperatures, over the entire measured (Q, E) range ($1 \text{ \AA}^{-1} < Q < 8 \text{ \AA}^{-1}$, $0 < E < 200 \text{ meV}$; $3 \text{ \AA}^{-1} < Q < 10 \text{ \AA}^{-1}$, $-100 < E < 900 \text{ meV}$). While the above spectral function agrees well with the data, we should point out that the assumption of a purely relaxational spin dynamics at finite temperatures and/or a Lorentzian function centered at ξ at low temperatures for mixed-valence materials cannot be justified physically. Such a model allows energy transfer from the system extended to indefinitely high values (or, a relaxational response at zero time), which is unphysical. In reality there must exist a cutoff at a finite energy, which of course is an important quantity to determine experimentally. From the present measurements made at temperatures between 100 and 200 K we find no evidence of the cutoff up to $\sim 200 \text{ meV}$ (see Fig. 5). At $T = 10 \text{ K}$ the tail of the inelastic peak extends to about 500 meV. At higher energies, corresponding to large Q values at a fixed scattering angle, the observed intensity falls off rapidly because of the form factor (see Fig. 6). Consequently, no conclusion can be made on the detailed line shape of the spectra above 500 meV. To reach energy transfer greater than 500 meV and yet maintain a small Q value, the experiment has to be done at small scattering angles ($< 5^\circ$) and with a much higher incident neutron energy ($\geq 10 \text{ eV}$). Such experimental configurations have not yet been fully exploited in the techniques of neutron spectroscopy using pulsed sources.

The Lorentzian amplitudes in the fit of Eq. (10) provide an estimate of the single-site f -electron static susceptibility as obtained from the neutron data. As discussed in the preceding section, the use of a standard vanadium sample allows the measurement of the magnetic scattering cross section in absolute units (mb per steradian per meV per Ce atom). From Eqs. (7) and (9) the single-site susceptibility, $\chi_0(T)$ in units of emu/mole Ce, is given by

$$\chi_0(T) = \frac{\pi N_A \mu_B^2}{2c} [A(T) + 2B(T)], \quad (11)$$

where N_A is Avogadro's number, $c = 0.74$ is the concentration of Ce in the alloy, and the Lorentzian amplitudes are in meV. The $\chi_0(T)$ determined from Eq. (11) may not be equal to the measured bulk susceptibility for the following reasons.

(i) The functional form (10) is not rigorously correct for the reasons stated above.

(ii) If the f sites are interacting, the bulk susceptibility per atom is not the same as the average single-site susceptibility. The former is given by $\lim_{q \rightarrow 0} \chi(\mathbf{q}, 0, T)$, while the latter is given by averaging over all \mathbf{q} .

(iii) There are contributions to the bulk susceptibility from the conduction electrons.

The static susceptibility deduced from Eq. (11) and its temperature dependence are given in Table I, together with the bulk susceptibility²⁴ for a $\text{Ce}_{1-x}\text{Th}_x$ sample with a value of $x = 0.269$, close (but not identical) to the concentration of the present sample. In view of the simplicity of the relaxational model adapted, the absolute agreement between the neutron and bulk measurements at all temperatures is quite good. We may thus conclude that

none of the factors (i)–(iii) enumerated above constitutes an important effect on the susceptibility, or else they give rise to compensating errors.

The neutron scattering result also provides information on the average occupation of the $4f$ shell in the α and γ phases. From Eqs. (5) and (6), we obtain

$$\langle n_f \rangle = \frac{3}{2} \frac{1}{g_f^2 J(J+1)} \frac{1}{|f(Q)|^2} \frac{1}{N} \int_{-\infty}^{+\infty} S_{\text{mag}}^{\text{av}}(Q, E) dE. \quad (12)$$

In practice, one cannot integrate over all E due to lack of data and hence one may define

$$\langle n_f \rangle_{\text{eff}} = \frac{3}{2} \frac{1}{g_f^2 J(J+1)} \frac{1}{|f(Q)|^2} \frac{1}{N} \int_{-E_0}^{E_1} S_{\text{mag}}^{\text{av}}(Q, E) dE, \quad (12')$$

where E_0, E_1 are suitable cutoff energies determined by the experimental data or the chosen theoretical model. $\langle n_f \rangle_{\text{eff}}$ may be regarded as the number of f electrons per site taking part in the observed frequency range of spin fluctuations. Using Eq. (12') we have determined $\langle n_f \rangle_{\text{eff}}$ from the data by choosing $-E_0$ to be -100 meV (negative E corresponds to neutron energy gain) and E_1 to be 230 meV . The results were obtained by numerically integrating the magnetic scattering over the specified energy range, and are shown in Table II. Here, $\langle n_f \rangle_{\text{eff}}$ is expressed as the f occupation per Ce atom rather than per lattice site. This obtained $\langle n_f \rangle_{\text{eff}}$ should be considered as the lower limit of $\langle n_f \rangle$ because of the truncated energy range used in the integration. In fact, neutron scattering data³⁰ of other cerium mixed-valence compounds indicate that reasonable $4f$ occupancy can be obtained by integrating the fitted Lorentzian up to about 2 eV. In Table II we also included the $\langle n_f \rangle_{\text{eff}}$ estimated by Eq. (12') with $S_{\text{mag}}^{\text{av}}$ replaced by the fitted Lorentzian (see Table I) and with E_1 extended to 0.5, 1, and 2 eV. As can be seen, in the γ phase the $4f$ occupancy becomes very close to 1, which is consistent with those determined from other measurements.^{12–17,24} In the α phase, on the other hand, the $\langle n_f \rangle_{\text{eff}}$ obtained is unphysically large. This indicates that in the α phase the pure relaxational model may no longer be a valid representation of the spin dynamics in this material. In the case of $T = 10 \text{ K}$, we obtained an $\langle n_f \rangle_{\text{eff}}$ of 0.76 by numerically integrating the magnetic scattering from 50 to 500 meV. This value is in good agreement with that deduced from photoemission experiments.¹⁸

Finally, we turn to the discussion of the width parameter $\Gamma_1(T)$, also listed in Table I. We find that $\Gamma_1(T)$ changes from about 16 meV in the γ phase to about 110 meV in the α phase. The large value of $\Gamma_1(T)$ in the α phase could not be determined accurately in the earlier neutron scattering experiment²⁴ because it exceeds the energy range of that measurement. The almost order-of-magnitude increase in $\Gamma_1(T)$ in the α phase is consistent with a sudden increase of the hybridization involving f and conduction electrons for $T < T_0$.

TABLE II. Parameters obtained from neutron data for $\text{Ce}_{0.74}\text{Th}_{0.26}$ and those from photoemission experiment¹⁸ on Ce metal.

	T (K)	δ (meV)	Neutron				Δ (meV)
			$E_1=230$	$E_1=500$	$\langle n_f \rangle_{\text{eff}}$ (meV) $E_1=1000$	$E_1=2000$	
α phase	10	138 ± 6		0.76			229
	100	110 ± 6	0.36	0.64	0.92	1.21	
	140	63 ± 4	0.46	0.69	0.90	1.12	
γ phase	155	25 ± 2	0.60	0.74	0.89	1.03	
	200	16 ± 1	0.65	0.73	0.83	0.92	
Photoemission							Δ (meV)
	T (K)	δ (meV)	$\langle n_f \rangle_{\text{eff}}$ (meV)				
α phase	10	26	~ 0.75				105
γ phase	150	5	~ 0.97				82

V. SUMMARY AND DISCUSSION

We have extended inelastic neutron scattering measurements on the polycrystalline mixed-valence alloy $\text{Ce}_{0.74}\text{Th}_{0.26}$ to higher energy transfers than previously, i.e., up to ~ 250 meV for $100 \leq T \leq 200$ K, ~ 900 meV for $T = 10$ K. The paramagnetic response across the cerium $\gamma \rightarrow \alpha$ valence transition in this alloy was studied in detail at 10, 100, 140, 155, and 200 K. The obtained magnetic scattering functions are shown in Figs. 5 and 6. They consist of a single broad peak, which is well fitted by a simple functional form given by Eq. (10). This peak shifts to higher energies and broadens as the temperature is lowered. Within experimental precision, we find no evidence of additional inelastic peaks due to crystal-field excitations. As the temperature decreases across the transition temperature, the magnetic intensity drops sharply, accompanied by an abrupt broadening of the linewidth corresponding to a spin-fluctuation energy much higher than the thermal energy. The static single-site susceptibility obtained by the Kramers-Kronig analysis agrees well with the bulk susceptibility. The \mathbf{Q} dependence of the intensity in both the γ and α phases within the temperature range from 100 to 200 K enables us to characterize it as from Ce^{3+} free ions, although no information on the directional \mathbf{q} dependence of the dynamical susceptibility can be obtained in the present study. The value for the average f -shell occupation number, evaluated by summing the observed intensities at 10 K from 50 to 500 meV and by integrating the fitted Lorentzian functions in the γ phase up to 2 eV, follows closely the valence behavior estimated by other methods. We are unable to unambiguously observe a cutoff energy in the excitation spectrum of $\text{Ce}_{0.74}\text{Th}_{0.26}$. Qualitatively, these results support the picture of the $\gamma \rightarrow \alpha$ transition as being associated with a sudden change in hybridization width and only a subtle change in $\langle n_f \rangle$, which is never much less than 1, i.e., we are in the Kondo rather than the strongly intermediate valence regime for this material at all temperatures.

Recently, results using polarized neutrons for pure ceri-

um³² have been presented. While the energy resolution and counting statistics in this experiment were insufficient to reveal the energy structure seen up to 200 meV in $S_{\text{mag}}(E)$, they indicated an increase in scattering at around ~ 200 meV at low temperature. This may be the spin-orbit splitting peak, which as also seen in recent photoemission experiments¹⁸ at 280 meV. These results are qualitatively in agreement with our present data on $\text{Ce}_{0.74}\text{Th}_{0.26}$. Note that the formalism given in Sec. IV applied only to the lower-lying excitation spectrum with the $J = \frac{5}{2}$ multiplet.

As stated previously, there is currently no simple analytical form available for the dynamical susceptibility from a theoretical treatment of the Kondo impurity problem at finite temperature. Kuramoto and his co-workers²⁰ have, however, formulated a theory for the dynamical susceptibility for a Ce impurity and carried out numerical calculations for certain parameter values and temperatures. The temperature dependence of the dynamical susceptibility of their calculations is in qualitative agreement with the results of our neutron scattering experiment. On the other hand, in the high-temperature γ phase the calculated quasielastic widths are too small by a factor of ~ 4 . At low temperatures, they predict a peak in $\text{Im}\chi(E)/E$ at a finite E of approximately 45 meV, which is at an energy about three times smaller than the observed peak position of our data at 10 K (see Fig. 6). This discrepancy may be due to the choice of parameters in their calculations or it may also arise from the dispersive broadening induced by the \mathbf{q} dependence left out in single-impurity-type treatments of the problem.

Since the theory of Gunnarsson and Schönhammer¹⁹ has been used to analyze the results of photoemission and other electronic spectroscopy measurements,¹⁸ it is of interest to see if one may apply it to discuss the present results. The theory is basically a ground-state ($T=0$) theory for a single f impurity in the metal. One may fairly easily obtain the results from this theory in the $U \rightarrow \infty$ limit to leading order in $1/N_f$, where N_f is the degeneracy of the f multiplet ($N_f=6$ for $J = \frac{5}{2}$). The result is

$$\begin{aligned}
S_{\text{mag}}(Q, E)_{\text{impurity}} &= |f(Q)|^2 g_f^2 (1 - \langle n_f \rangle)^{\frac{2}{3}} J(J+1) \frac{\Delta}{\pi E^2}, \quad E > \delta, \\
&= 0, \quad E < \delta.
\end{aligned} \tag{13}$$

Here $\Delta = \pi N_f V^2$, where V is the average hybridization energy and δ is the quantity which measures the lowering of the f -shell energy due to hybridization, or the quantity $k_B T_K$, where T_K is the Kondo temperature. This result applies only for $T=0$ and neglects spin-orbit splitting, but yields the correct values for both the static susceptibility and $\langle n_f \rangle$ in this approximation, as can be easily verified by using the sum rules (7) and (12) given in this paper and comparing with Eqs. (C4) and (8.6) of Ref. 19.

This simple result implies that at $T=0$, $S_{\text{mag}}(E)$ should have a threshold at $E=\delta$, with an E^{-2} tail for higher energies. Considerable modifications³³ of the above expression occur however, when crystal-field and spin-orbit splitting are taken into account. Therefore, although in the present experiment the deduced $S_{\text{mag}}^{\text{av}}$ at 10 K shows a thresholdlike behavior at ~ 138 meV (see Fig. 6), we feel that a detailed comparison of the line shape with theory is not warranted at this time. If we assume that the peak shape of Eq. (13) applies, at higher temperatures, with some additional broadening, then this implies that the peak in $S_{\text{mag}}(E)$ is approximately at δ , the Kondo energy. Thus in the present results, we find that δ goes from a value of ~ 16 meV at 200 K to ~ 138 meV at 10 K. These values are about 3 to 5 times larger than those deduced by Patthey *et al.*¹⁸ from the low-frequency part of their photoemission spectrum for pure γ - and α -cerium, respectively. If we assume an $\langle n_f \rangle$ of 0.76 deduced from the 10-K data, and substitute in the formula for δ (Ref. 19)

$$\frac{\langle n_f \rangle}{1 - \langle n_f \rangle} = \frac{N_f \Delta}{\pi \delta}, \tag{14}$$

we obtain a value of ~ 229 meV for Δ in the α phase. This is about twice of the value obtained from the photoemission data in α Ce.¹⁸ This discrepancy is not surprising because, as it was pointed out in Ref. 19, Δ depends very sensitively on $\langle n_f \rangle$, according to Eq. (14). One may also check the relation between Δ , χ , and $\langle n_f \rangle$ given by Gunnarsson and Schönhammer.¹⁹ Using $\langle n_f \rangle = 0.76$ and χ (Ref. 24) (in appropriate units) at 10 K, one obtains from their calculation (see Eq. 8.7 and Fig. 14 of Ref. 19, which includes spin-orbit splitting) a value for Δ of 148 meV, to be compared with the values mentioned above (see also Table II).

The ground state of a mixed-valence system, under the single-impurity model,^{34,35,19} is a singlet in which hybridi-

zation admixes the magnetic configuration f^n . Its polarizability gives rise to a spin susceptibility which exhibits Curie-Weiss behavior at high temperatures, followed by a broad maximum at lower temperatures, and then levels off to a constant value as $T \rightarrow 0$ K. At $T=0$ K the susceptibility is given by^{19,35}

$$\chi_0(0) = N_A \mu_B^2 g_f^2 J(J+1) \frac{\langle n_f \rangle}{3 |E_0 - \epsilon_f|}, \tag{15}$$

where E_0 is the renormalized energy of the f^{n-1} configuration and ϵ_f is the bare energy level of the f shell. If we identify the quantity $|E_0 - \epsilon_f|$ with δ , the lowering of the f -shell energy that tends to stabilize the ground state, this will provide a comparison of the low-temperature susceptibility obtained by the neutron measurements with the theory. Using $\delta = 138$ meV obtained from the fit of a Lorentzian to the data at 10 K (see Fig. 6), we find, from the above equation, $\chi_0(0) = 0.51 \times 10^{-3}$ emu/mole Ce. This value is in excellent agreement with the bulk susceptibility²⁴ of 0.54×10^{-3} emu/mole Ce. Furthermore, the coefficient of electronic specific heat is given by the theory³⁵ as

$$\gamma = N_A \pi^2 k_B \frac{\langle n_f \rangle}{3 |E_0 - \epsilon_f|}. \tag{16}$$

From the neutron result and Eq. (16) we obtain $\gamma = 13.1$ mJ/mole Ce/K², to be compared with $\gamma = 12.8$ mJ/mole Ce/K² for α Ce (Ref. 36) and 17.4 mJ/mole Ce/K² for Ce_{0.8}Th_{0.2}.³⁷ Thus, in a semiquantitative sense, the model is fairly consistent with the neutron scattering data. This affords an interesting comparison of the same model as applied to both neutron and electronic spectroscopy from these systems.

Finally, we should mention that there may be features in the spectrum due to coherence effects in the lattice (e.g., excitations across hybridization gaps^{38,39} which are smeared over and lost in the polycrystalline results). Unfortunately, assessment of these effects by neutron experiments has to await the availability of large, good quality, single-crystal specimens and further development in instrumental sensitivity and neutron source intensity in the future.

ACKNOWLEDGMENTS

One of us (S.K.S.) wishes to acknowledge the support of the Guggenheim Foundation during the period in which this work was carried out. Works at IPNS of Argonne National Laboratory and at Brookhaven National Laboratory are supported by the Division of Materials Science, U.S. Department of Energy, respectively, under Contract Nos. W-31-109-ENG-38 and DE-AC02-76CH00016.

*Deceased.

¹W. H. Zachariasen, Phys. Rev. **76**, 301 (1949).

²L. Pauling, J. Chem. Phys. **18**, 145 (1950).

³B. Coqblin and A. Blandin, Adv. Phys. **17**, 281 (1968).

⁴R. Ramirez and L. M. Falicov, Phys. Rev. B **3**, 2485 (1971).

⁵L. L. Hirst, Phys. Rev. B **15**, 1 (1977).

⁶B. Johansson, Philos. Mag. **30**, 469 (1974).

⁷D. C. Koskenmaki and K. A. Gschneidner, Jr., in *Handbook on the Physics and Chemistry of the Rare Earths*, edited by K. A. Gschneidner and L. Eyring (North-Holland, Amsterdam,

- 1978), Vol. 1, Chap. 4.
- ⁸A. S. Edelstein, *Phys. Rev. Lett.* **20**, 1348 (1968).
- ⁹J. M. Lawrence, P. S. Riseborough, and R. D. Parks, *Rep. Prog. Phys.* **44**, 1 (1981).
- ¹⁰J. W. Allen and R. M. Martin, *Phys. Rev. Lett.* **49**, 1106 (1982).
- ¹¹M. Lavagna, C. Lacroix, and M. Cyrot, *J. Phys. F* **13**, 1007 (1983).
- ¹²D. R. Gustafson, J. D. McNull, and L. D. Roelling, *Phys. Rev.* **183**, 435 (1969); R. F. Gempel, D. R. Gustafson, and J. D. Willenberg, *Phys. Rev. B* **5**, 2082 (1972).
- ¹³H. Wher, K. Knorr, F. N. Gyax, A. Schlenk, and W. Studer, *Phys. Rev. B* **24**, 4041 (1981).
- ¹⁴E. Wuilloud, H. R. Moser, W. D. Schneider, and Y. Baer, *Phys. Rev. B* **27**, 7354 (1983).
- ¹⁵D. M. Wieliczka, J. H. Weaver, D. W. Lynch, and C. G. Olson, *Phys. Rev. B* **26**, 7056 (1982).
- ¹⁶J. W. Allen, S. J. Oh, I. Lindau, J. M. Lawrence, L. I. Johansson, and S. B. Hagstrom, *Phys. Rev. Lett.* **46**, 1100 (1981).
- ¹⁷U. Kornstädt, R. Lässer, and B. Lengeler, *Phys. Rev. B* **21**, 1898 (1980).
- ¹⁸F. Patthey, B. Delley, W. D. Schneider, and Y. Baer, *Phys. Rev. Lett.* **55**, 1518 (1985).
- ¹⁹O. Gunnarsson and K. Schönhammer, *Phys. Rev. B* **28**, 4315 (1983).
- ²⁰Y. Kuramoto and H. Kojima, *Z. Phys. B* **57**, 95 (1984); Y. Kuramoto, *ibid.* **53**, 37 (1980); H. Kojima, Y. Kuramoto, and M. Tachiki, *Z. Phys.* **54**, 293 (1984).
- ²¹K. A. Gschneidner, Jr., R. O. Elliott, and R. R. McDonald, *J. Phys. Chem. Solids* **23**, 555 (1962); **23**, 1191 (1962); **23**, 1201 (1962).
- ²²J. M. Lawrence, M. C. Croft, and R. D. Parks, *Phys. Rev. Lett.* **36**, 1332 (1975).
- ²³B. H. Grier, R. D. Parks, S. M. Shapiro, and C. F. Majkrzak, *Phys. Rev. B* **24**, 6242 (1981).
- ²⁴S. M. Shapiro, J. D. Axe, R. J. Birgeneau, J. M. Lawrence, and R. D. Parks, *Phys. Rev. B* **16**, 2225 (1977).
- ²⁵C.-K. Loong, *J. Appl. Phys.* **57**, 3772 (1985).
- ²⁶See references in Proceedings of the Conference on High Energy Excitations in Condensed Matter, February 13–15, 1984, edited by R. A. Silver, Los Alamos National Laboratory Report No. LA-10227-C (unpublished).
- ²⁷D. L. Price, J. M. Carpenter, C. A. Pelizzari, S. K. Sinha, I. Bresof, and G. E. Ostrowski, in Proceedings of the 6th Meeting of the International Collaboration on Advanced Neutron Sources, 28 June–2 July 1982, Argonne National Laboratory Report No. ANL-82-80 (1983), p. 207 (unpublished).
- ²⁸J. R. D. Copley, D. L. Price, and J. M. Rowe, *Nucl. Instrum. Methods* **107**, 501 (1973).
- ²⁹C. Stassis, W. H. Deckman, B. N. Harmon, J. D. Desclaux, and A. J. Freeman, *Phys. Rev. B* **15**, 369 (1977).
- ³⁰E. Holland-Moritz, D. Wohlleben, and M. Loewenhaupt, *Phys. Rev. B* **25**, 7482 (1982).
- ³¹D. L. Price and K. Sköld, in *Methods of Experimental Physics-Neutron Scattering in Condensed Matter Research*, edited by K. Sköld and D. L. Price (Academic, New York, 1986), Vol. 23A, Chap. 1.
- ³²G. Fillion, R. M. Galera, D. Givord, J. Pierre, J. Schweizer, and C. Vettier, *J. Appl. Phys.* **57**, 3179 (1985).
- ³³O. Gunnarsson and K. Schönhammer, in *Theory of Heavy Fermions and Valence Fluctuation*, edited by T. Kasuya and T. Sass (Springer-Verlag, New York, 1985), p. 100.
- ³⁴C. M. Varma and Y. Yafet, *Phys. Rev. B* **13**, 2950 (1976).
- ³⁵T. V. Ramakrishnan and K. Sur, *Phys. Rev. B* **26**, 1798 (1982).
- ³⁶D. C. Koskimaki and K. A. Gschneidner, Jr., *Phys. Rev. B* **11**, 4463 (1975).
- ³⁷R. A. Elenbaas, C. J. Schinkel, and E. Swakman, *J. Phys. F* **9**, 1261 (1979).
- ³⁸A. J. Fedro and S. K. Sinha, in *Valence Fluctuations in Solids*, edited by L. M. Falicov, W. Hanke, and M. B. Maple (North-Holland, Amsterdam, 1981), p. 321; also in *Moment Formation in Solids*, edited by W. J. Buyers (Plenum, New York, 1984), p. 135.
- ³⁹D. L. Huber, *Phys. Rev. B* **28**, 860 (1983).